St-Pierre, Luc; Martorell, Ned J.; Pinho, Silvestre T.

Stress redistribution around clusters of broken fibres in a composite

Published in:
Composite Structures

DOI:
10.1016/j.compstruct.2017.01.084

Published: 15/05/2017

Document Version
Peer-reviewed accepted author manuscript, also known as Final accepted manuscript or Post-print

Stress redistribution around clusters of broken fibres in a composite

Luc St-Pierre*, Ned J. Martorell, Silvestre T. Pinho

Department of Aeronautics, Imperial College London, South Kensington, London SW7 2AZ, UK

Abstract

A key aspect of the longitudinal tensile failure of composites is the stress redistribution that occurs around broken fibres. Work on this topic has focussed mainly on the stress field surrounding a single broken fibre; however, this is an important limitation as unstable failure in carbon fibre bundles occurs when a cluster of about 16 or more broken fibres is formed. Therefore, we have developed a detailed Finite Element (FE) model to investigate how stress redistribution varies with the number of broken fibres in a cluster. The results show that both the recovery length and stress concentration factor increase significantly with increasing number of broken fibres in a cluster. We have also developed an analytical model, suitable to be included in existing or new fibre bundle models, that captures how the recovery length and stress concentration factor vary with the broken cluster size, and validated its predictions against our FE simulations. Finally, we extended our FE model to predict the survival probability of fibre bundles using Monte Carlo simulations, and found that these predictions were in good agreement with experimental and analytical results on microcomposites.

Keywords: Carbon fibres, Finite element analysis (FEA), Stress concentrations, Monte Carlo simulations

1. Introduction

Longitudinal tensile failure of composites is a complex process governed by: (i) variations in strength between each fibre and (ii) the stress redistribution that occurs around broken fibres [1, 2]. While strength variations can be quantified using single fibre tensile tests, insights

*Corresponding author. Present address: Department of Mechanical Engineering, Aalto University, 02150 Espoo, Finland.

Email addresses: luc.st-pierre@aalto.fi (Luc St-Pierre), silvestre.pinho@imperial.ac.uk (Silvestre T. Pinho)

on stress redistribution rely essentially on modelling efforts. Many early analytical models were developed to predict the stress field around clusters of broken fibres: first for 1D [3, 4] and then for 2D [5, 6] arrays of fibres embedded in a linear elastic matrix. However, it is challenging to include the effect of matrix plasticity in these models and, consequently, analytical studies of stress redistribution considering clusters of broken fibres and a plastic matrix have been limited to 1D fibre packings only [7, 8].

This limitation was alleviated by the development of Finite Element (FE) models to study stress redistribution. This approach allowed researchers to represent 1D [9], square [10–14], hexagonal [15–17] and random [18, 19] fibre arrangements, and to model the matrix as an elastic-plastic material [9–11, 13–16, 18]. With the exception of Blassiau et al. [12–14], who have considered different conditions of diffuse damage, most FE studies have analysed the stress redistribution that occurs around a single broken fibre. However, this is an important limitation as there is growing experimental [20, 21] and analytical [22] evidence that unstable failure of a carbon fibre/polymer matrix bundle occurs when a cluster of approximately 16 or more broken fibres is formed. Hence, there is a need to quantify how stress redistribution varies with the number of broken fibres in a cluster, and this will be investigated in the first part of the paper using both analytical and FE modelling.

Accurately representing how stress redistribution varies with the size of the broken cluster is a critical component of models predicting the strength of fibre bundles, especially for those using a two-step simulation technique [18, 23–25]. With this approach, a deterministic model is first used to calculate the stress field around a single broken fibre. Second, a Monte Carlo simulation is performed in which fibres are assigned a stochastic strength and when a fibre breaks, the stress redistribution is defined by superposition of the solution obtained in the first step. A fundamental assumption of this technique is that stress redistribution around a cluster of broken fibres can be obtained simply by superposition of the stress field around a single broken fibre. In addition to approximating the stress concentration factor, a crucial implication of the superposition technique is that the recovery length does not change with the number of broken fibres in a cluster. Therefore, replacing this superposition method by a precise representation of how stress redistribution varies with the number of broken fibres in a cluster would be valuable for this two-step modelling approach.

Alternatively, fibre bundle strength distributions can be predicted analytically. Most analytical models assume an idealised stress redistribution: when a fibre breaks, its load is redistributed either (i) equally between all surviving fibres (equal or global load sharing [26, 27]) or (ii) locally to the closest surviving fibres only (local load sharing [28, 29]). Models can also be based on a hierarchical build-up of the failure process [22]; this approach is computationally very efficient and the predictions were found to compare favourably with experimental results on several composites in the literature.

Finally, other researchers have predicted the strength of fibre bundles using Monte Carlo FE simulations where (i) the fibres are interconnected by a network of shear springs representing the matrix [30, 31] or (ii) both the fibres and matrix are modelled with continuum elements [32]. The latter approach is computationally demanding, which limits the analysis to very small volumes and consequently, no comparison with experiments could be presented in [32]. Therefore, in the second part of this paper, we present computationally efficient Monte Carlo FE simulations, where the fibres are modelled with truss elements and the matrix is meshed with continuum elements. We validate our approach by comparing our predictions to experiments on microcomposites [33, 34] and to analytical predictions [22].

This article is organised as follows. First, Section 2 focuses on the stress redistribution around clusters of broken fibres and contains: analytical predictions for the recovery length and stress concentration factor; a description of the FE model developed and a comparison between analytical and FE predictions. Second, Section 3 presents the Monte Carlo FE simulations and includes a description of the modelling approach and a comparison between measured and predicted survival probabilities for two different microcomposites.

2. Stress redistribution around broken fibres

The fibre bundle considered to analyse stress redistribution is illustrated in Fig. 1: it consists of a square arrangement of fibres and contains a cluster of broken fibres at its centre. Recent results [19] show that the fibre arrangement (hexagonal, square or random) does not significantly affect the stress concentration factor. All breaks are considered to be on the same plane, see Fig. 1. This is based on SEM images of fracture surfaces [35] and recent x-ray tomographic observations of incipient failure which showed that 70% of clusters analysed had

fibres broken in the same plane [25].

2.1. Analytical predictions

In this section, we present analytical equations to predict how: (i) the recovery length varies with the number of broken fibres in a cluster and (ii) the stress concentration factor varies with the number of broken fibres and the distance from the broken cluster. These analytical predictions will be compared to FE simulations in Section 2.3.

2.1.1. Recovery length

Consider the fibre bundle illustrated in Fig. 1: a total of n_t fibres are packed in a square arrangement with a regular spacing $s = \sqrt{\pi/V_\mathrm{f}}\phi/2$, defined by the fibre diameter ϕ and the fibre volume fraction V_f. When the fibres are loaded in tension by a remote fibre stress σ^∞, the cluster of n_b broken fibres will transfer its load to the neighbouring fibres by shearing the resin. Assuming a rigid perfectly-plastic resin with a shear strength τ_y, this load transfer will occur over a recovery length [22]:

$$l_\mathrm{e} = \frac{n_\mathrm{b} A_\mathrm{f} \sigma^\infty}{C\tau_\mathrm{y}}, \quad \text{with} \quad A_\mathrm{f} = \frac{\pi\phi^2}{4} \quad \text{and} \quad C = 4s\sqrt{n_\mathrm{b}} = 2\phi\sqrt{\frac{\pi n_\mathrm{b}}{V_\mathrm{f}}}. \tag{1}$$

The shape of the shear-lag perimeter C is illustrated in Fig. 1. Different shapes have been considered by Pimenta and Pinho [22], but they found that the choice of shear-lag perimeter had a reduced influence on the predicted strength of the bundle.

2.1.2. Stress redistribution

The problem of stress distribution is easier to represent using polar coordinates, with the origin positioned at the centre of the broken bundle, see Fig. 1. We can define two equivalent radii, one for the entire bundle r_t and a second one for the broken cluster r_b, given as

$$\pi r_\mathrm{t}^2 = n_\mathrm{t} s^2 \Rightarrow r_\mathrm{t} = \sqrt{\frac{n_\mathrm{t}}{\pi}} s = \sqrt{\frac{n_\mathrm{t}}{V_\mathrm{f}}} \frac{\phi}{2} \quad \text{and} \tag{2}$$

$$\pi r_\mathrm{b}^2 = n_\mathrm{b} s^2 \Rightarrow r_\mathrm{b} = \sqrt{\frac{n_\mathrm{b}}{\pi}} s = \sqrt{\frac{n_\mathrm{b}}{V_\mathrm{f}}} \frac{\phi}{2}. \tag{3}$$

Before their failure, the broken fibres carried a total force that can be expressed as

$$\Delta F = \pi r_{\mathrm{b}}^2 V_{\mathrm{f}} \sigma^{\infty}, \tag{4}$$

which needs to be redistributed to unbroken fibres. To choose an appropriate stress redistribution profile, we first examine the solutions of similar problems. Consider a cylinder loaded in tension containing either a penny-shaped crack or a spherical cavity, both of radius a. For the penny-shaped crack, the tensile stress field scales as $(a/r)^{1/2}$ [36], whereas for the spherical cavity it scales as $A(a/r)^3 + B(a/r)^5$, where A and B are two constants [37]. Based on these two solutions, we anticipate that the stress redistribution around a cluster of broken fibres will take a similar power form: $(r_{\mathrm{b}}/r)^{\alpha}$, where the value of the exponent α will be determined later. Hence, we hypothesise that the stress concentration factor, as a function of r, can be written as

$$k(r) = \frac{\sigma}{\sigma^{\infty}} = 1 + \lambda \left(\frac{r_{\mathrm{b}}}{r}\right)^{\alpha}. \tag{5}$$

For a given value of α, the constant λ can be solved by applying equilibrium:

$$\Delta F = \pi r_{\mathrm{b}}^2 V_{\mathrm{f}} \sigma^{\infty} = \int_{r_{\mathrm{b}}}^{r_{\mathrm{t}}} (\sigma - \sigma^{\infty}) V_{\mathrm{f}} 2\pi r dr, \tag{6}$$

which gives

$$\lambda = \frac{1}{2\ln(r_{\mathrm{t}}/r_{\mathrm{b}})} \quad \text{for } \alpha = 2 \quad \text{and} \quad \lambda = \frac{(2-\alpha) r_{\mathrm{b}}^{2-\alpha}}{2(r_{\mathrm{t}}^{2-\alpha} - r_{\mathrm{b}}^{2-\alpha})} \quad \text{for } \alpha \neq 2. \tag{7}$$

Therefore, Eq. (5) can be used to predict the stress concentration factor $k(r)$ for a given value of α, which will be determined below from the FE results. Finally, the closest fibre to the broken cluster experiences the maximum stress concentration factor $k_{\max}$ given by

$$k_{\max} = k(r = r_{\mathrm{c}}) = 1 + \lambda \left(\frac{r_{\mathrm{b}}}{r_{\mathrm{c}}}\right)^{\alpha} \quad \text{with} \quad r_{\mathrm{c}} = \frac{s(\sqrt{n_{\mathrm{b}}} + 1)}{2}, \tag{8}$$

where r_{c} is the distance from the centre of the broken cluster to the closest surviving fibre. The expression for r_{c} given in Eq. (8) is exact for odd values of n_{b}, but approximate for even numbers of broken fibres.

2.2. Description of the Finite Element model

All simulations analysing stress redistribution were performed using the implicit solver of the commercially available FE code Abaqus (version 6.14). The geometry, mesh, boundary conditions and material properties employed are described below.

2.2.1. Geometry and mesh

All bundles considered were made of carbon fibres, of diameter $\phi = 5\,\mu\text{m}$, that were squarely packed with a regular spacing $s = \sqrt{\pi/V_\text{f}}\phi/2 = 5.7\,\mu\text{m}$, corresponding to a fibre volume fraction $V_\text{f} = 60\,\%$, see Fig. 2. The total number of fibres n_t was varied from 16 to 900, but all bundles had a square cross-section (with $\sqrt{n_\text{t}}$ rows and columns of fibres) and a half-length $L = 0.75\,\text{mm}$ (which was significantly longer than the recovery length in all cases).

The fibres were discretised using 2-node linear truss elements (T3D2 in the Abaqus library), whereas the resin was meshed with 8-node linear brick elements with reduced integration and hourglass control (C3D8R in the Abaqus library). Constraint equations were used to represent a perfect bonding between the fibres and matrix. This approach of modelling the fibres with truss elements is more efficient than using continuum elements, and is consistent with experimental fibre strength characterisation which considers fibres to behave as one-dimensional entities. Both the fibres and matrix had a mesh size of $2\phi = 10\,\mu\text{m}$ along the x-direction, and the matrix had a structured mesh in the y-z plane with two elements between fibres, see Fig. 2. A convergence analysis revealed that further mesh refinement had a negligible effect on both the recovery length and the maximum stress concentration factor.

The FE simulations performed in this study do not include debonding of the fibre-matrix interface. While interfacial debonding is often observed in single fibre fragmentation tests, there is no evidence of debonding occurring in composites with thousands or millions of fibres [2]. In addition, recent x-ray tomography images [21, 25] suggest that debonding may not occur during the formation of clusters; in fact, the prevalence of planar clusters appear to be incompatible with the formation of splits after each fibre breaks. In any case, debonding could potentially be included in the FE model by adding cohesive elements at the fibre-matrix interface. A few numerical studies have shown that debonding increases the recovery length

and slightly reduces the stress concentration factor [9, 16, 31].

2.2.2. Boundary conditions

Only half of the bundle's length was modelled by applying symmetry boundary conditions at $x = 0$, see Fig. 2. A displacement u_x was prescribed at $x = L$. A cluster containing $n_\mathrm{b} = 1$ to 36 broken fibres was included at the centre of the bundle by removing the symmetric boundary conditions and the corresponding constraint equations at $x = 0$ for all broken fibres. In each model, the broken cluster considered was square with $\sqrt{n_\mathrm{b}}$ rows and columns of broken fibres.

In reality, clusters of broken fibres are formed as loading is increased, but the boundary conditions detailed above assume that all fibres are broken before loading is applied. This assumption is inconsequential for elastic models, but it could, in principle, have a significant effect on the results when plasticity is included. Xia et al. [15] investigated this problem for polymer and aluminium matrix composites, and their results indicate that the assumption of an initial broken cluster is acceptable for carbon fibre reinforced polymers such as the one considered in this study.

2.2.3. Material properties

The material properties employed are summarised in Table 1 and were chosen to represent the T800H/3631 carbon fibre prepreg. The T800H carbon fibres were modelled as linear elastic whereas the 3631 epoxy was represented as a linear elastic perfectly-plastic solid in accordance with J2 flow theory.

The material models used for the fibres and matrix represent of course idealisations of reality and other approaches have also been considered in the literature. For example, Swolfs et al. [19] showed that modelling the fibres as transversely isotropic (instead of isotropic) results in higher stress concentrations; these results were obtained for fibres embedded in an elastic matrix and when matrix plasticity is included the effect of fibre anisotropy is reduced [15]. In the literature, the matrix has been modelled with a variety of constitutive behaviours such as linear elastic [12, 17, 19, 25], non-linear elastic [10], linear elastic perfectly-plastic [13, 14, 18] or linear elastic with linear strain hardening [38]. Results indicate that for the options enumerated above, matrix plasticity has a reduced effect on the stress concentration factor, but

leads to longer recovery lengths [2]. However, our knowledge of the matrix behaviour is based on pure tension, compression or shear tests done on bulk epoxy, and these experiments are unlikely to be representative of in situ conditions where a high stress triaxiality is present and high strain-rates may occur following a fibre break. Therefore, in the absence of representative in situ test data, we modelled the resin as a linear elastic perfectly-plastic solid, which is a reasonable compromise between simplicity and what is known of the resin's response in this problem.

2.3. Results and discussion

The results of FE simulations are presented in this section, and compared to the analytical predictions introduced earlier in Section 2.1. All results are shown for a remote fibre stress $\sigma^\infty = 4.3\,\text{GPa}$ (representative of the average measured strength of T800H carbon fibres [39]).

2.3.1. Stress profile

We begin by examining how the stress in a fibre varies along its length (x-direction) for the case of $n_\text{b} = 1$ broken fibre in a bundle of $n_\text{t} = 25$ fibres. The longitudinal tensile stress σ, normalised by the remote fibre stress $\sigma^\infty = 4.3\,\text{GPa}$, is plotted in Fig. 3 as a function of the distance from the break plane x, normalised by the fibre diameter $\phi = 5\,\mu\text{m}$. Results are shown for the broken fibre and its closest neighbour.

The stress in the broken fibre increases linearly up to $x/\phi \approx 12$. Subsequently, the stress increases up to $\sigma/\sigma^\infty = 1$ in a non-linear manner, which makes it difficult to identify clearly the recovery length. In this article, the linear portion of the stress profile was used to extrapolate the recovery length l_e as shown by the dashed line in Fig. 3. Other researchers [19, 26] have taken the recovery length as the distance where 90% of the remote stress is recovered, but both definitions were found to give similar results.

As shown in Fig. 3, the closest fibre to the broken cluster experiences the maximum stress concentration factor $k_\text{max} = \sigma_\text{max}/\sigma^\infty = 1.077$. This value is in good agreement with FE results reported in the literature: Nedele and Wisnom [17] found a value of 1.058 for a hexagonal fibre arrangement and Swolfs et al. [19] reported 1.075 for a square arrangement. We note that these two studies have used continuum elements to mesh the fibres whereas truss elements were employed here. Using truss elements allowed us to efficiently consider

significantly larger bundles than those previously reported in the literature; we modelled bundles with $n_t = 900$ fibres and $L = 0.75\,\text{mm}$ whereas results available in the literature were for at the most 125 fibres and a length of $0.14\,\text{mm}$ [19].

Now that both the recovery length l_e and the maximum stress concentration factor k_{max} are clearly defined, we proceed by examining how these quantities vary with the number of broken fibres n_b.

2.3.2. Recovery length

The recovery length l_e, normalised by the fibre diameter $\phi = 5\,\mu\text{m}$, is plotted in Fig. 4a as a function of the total number of fibres in the bundle n_t. Results are shown for selected numbers of broken fibres n_b and, as mentioned earlier, l_e is taken at a remote stress $\sigma^\infty = 4.3\,\text{GPa}$. The error bars in Fig. 4a show the minimum/maximum recovery length for all broken fibres in the cluster. The very small scatter indicates that defining l_e for the cluster as the average of all broken fibres is justifiable.

The results in Fig. 4a show clearly that the recovery length (i) increases with increasing number of broken fibres n_b and (ii) is insensitive to the bundle size n_t (provided that the bundle is sufficiently long). These FE results are compared to Eq. (1) in Fig. 4b, where l_e/ϕ is plotted as a function of the number of broken fibres n_b for the largest bundle considered with $n_t = 900$ fibres. There is an excellent agreement between the FE predictions and Eq. (1) for the wide range of n_b considered in this study.

Note that Eq. (1) can be particularly useful for models predicting the strength of fibre bundles. While some fibre bundle models [22] take into account the dependency of l_e with n_b, others [40, 41] assume that the recovery length is insensitive to the size of the broken cluster. The results in Fig. 4 show that this assumption significantly underestimates l_e, and this error would lead to overestimating the bundle strength. Implementing Eq. (1) in fibre bundle models would eliminate this error as it offers an efficient and accurate way to capture how l_e varies with n_b.

2.3.3. Maximum stress concentration factor

The maximum stress concentration factor k_{max}, defined as the highest value of k for all unbroken fibres, is plotted as a function of the total number of fibres in the bundle n_t in

Fig. 5a for different broken cluster sizes n_b. At first glance, the data is not as smooth as one would expect, especially for $n_b = 4$ to 16. This is because depending on the combinations of n_t and n_b, the centre of the broken cluster does not always coincide with the centre of the bundle (*e.g.* when $n_t = 16$ and $n_b = 4$ they coincide, but when $n_t = 25$ and $n_b = 4$, they do not).

The results in Fig. 5a show that k_{max} is sensitive to both the number of broken fibres n_b and the total number of fibres in the bundle n_t. For a given bundle size n_t, k_{max} increases with increasing number of broken fibres n_b. However, for a given broken cluster size n_b, the stress concentration factor k_{max} decreases with increasing bundle size n_t, until an asymptotic value is reached when $n_t \approx 25n_b$. The dependency of k_{max} upon the total number of fibres n_t has important implications: some FE predictions [10] of the stress concentration factor around a single broken fibre have been obtained with bundles containing 9 fibres, and the results in Fig. 5a indicate that considering such small bundles may overestimate k_{max}. However, if these results for $n_t = 9$ and $n_b = 1$ were generalised to be representative of clusters of broken fibres, then k_{max} would be underestimated.

The asymptotic value of k_{max}, for a large bundle with $n_t = 900$ fibres, is plotted as a function of the number of broken fibres n_b in Fig. 5b. The size of the broken cluster has a strong effect on the maximum stress concentration factor; for example, increasing n_b from 1 to 16 increases k_{max} from 1.06 to 1.17. The predictions of Eq. (8) are also included in Fig. 5b for comparison. These analytical predictions were obtained by setting the exponent $\alpha = 2$, and we show later in Section 2.3.4 how this value was obtained. Considering its simplicity, the analytical model captures reasonably well how k_{max} varies with n_b, especially for small values of n_b.

2.3.4. Stress redistribution

In the previous section, we examined how the maximum stress concentration factor k_{max} varies with the size of bundle and of the broken cluster. In this section, we take a closer look at the entire stress redistribution that occurs in the plane containing the broken cluster. The relative increase in stress experienced by each unbroken fibre is given by $k-1 = (\sigma-\sigma^\infty)/\sigma^\infty$ and is plotted in Fig. 6a as a function of the normalised distance r/s from the centre of the

broken cluster (see Fig. 1). Plots are in logarithmic scale and results are shown for different broken cluster sizes n_b inside a bundle of $n_t = 900$ fibres.

The results in Fig. 6a show that increasing the number of broken fibres n_b increases not only k_{max} but the entire k versus r/s curve. Using a logarithmic scale emphasises that, for a given value of n_b, $k-1$ decreases exponentially with increasing r/s, where the slope in logarithmic coordinates corresponds to the value of the exponent α in Eq. (5). A slope of $\alpha = 2$ offers a good fit to the results shown in Fig. 6a. Now that the value of the exponent α is set to 2, we can compare the predictions of the analytical model presented in Section 2.1.2 to the FE data shown in Fig. 6a. According to Eq. (5), all FE data should collapse on a single curve when plotted as $(k-1)/\lambda$ versus r/r_b. To test the accuracy of our analytical prediction, the data shown earlier in Fig. 6a is replotted using this new normalisation in Fig. 6b. Clearly, there is an excellent agreement between the FE results and the analytical predictions over the entire stress distribution and for the wide range of n_b considered in this study. Hence, Eq. (5) offers an efficient and accurate prediction of the stress redistribution around clusters of broken fibres.

3. Monte Carlo Finite Element predictions

3.1. Description of the Finite Element model

The FE model described in Section 2.2 was adapted to predict the survival probability of fibre bundles. These simulations are compared below to two different sets of experiments on microcomposites: the first set consists of four squarely packed AS4 carbon fibres in a blend of DER 331 and 732 epoxies (50:50) [33], whereas the second set has a hexagonal arrangement of seven IM6 carbon fibres embedded in a DER 331 epoxy [34].

The fibre bundles modelled had a length $L = 10\,\text{mm}$, as used in the experiments [33, 34]. All degrees-of-freedom were constrained to zero at $x = 0$, whereas a prescribed displacement was applied at $x = L$, see the reference frame introduced earlier in Fig. 2. The elements used and the mesh were the same as those described previously in Section 2.2 and are therefore mesh-converged.

The matrix was represented again as a linear elastic perfectly-plastic solid, but the fibres were modelled as linear elastic with failure (element deletion) when a maximum stress is

reached. The strength of each fibre element σ_{el} was assigned to follow a Weibull distribution and scale according to weakest link theory such as

$$S_{\mathrm{el}} = \exp\left[-\frac{L_{\mathrm{el}}}{L_0}\left(\frac{\sigma_{\mathrm{el}}}{\sigma_0}\right)^m\right] \quad \Rightarrow \quad \sigma_{\mathrm{el}} = \sigma_0\left[-\frac{L_0}{L_{\mathrm{el}}}\ln\left(S_{\mathrm{el}}\right)\right]^{\frac{1}{m}}, \tag{9}$$

where L_{el} is the element length; the survival probability S_{el} is a randomly generated number; and σ_0 and m are the Weibull scale and shape parameters obtained from single fibre tensile tests at a gauge length L_0. All material properties employed are summarised in Table 2, and these were all obtained from experiments [33, 34].

All computations were performed in Abaqus using the dynamic implicit solver with the quasi-static option. To ensure convergence of the solution, the matrix included Raleigh material damping where $\alpha_{\mathrm{m}} = 1.57\mathrm{e}7\,\mathrm{s}^{-1}$ and $\beta_{\mathrm{m}} = 1.06\text{e-}4\,\mathrm{s}$ are the mass and stiffness proportional factors, respectively. At the peak stress, the energy dissipated by damping was less than 3% of the total strain energy which indicates that damping helped convergence of the solution without compromising the results. It is worth noting that the fibre element deletion process accounts for only 5% of the energy dissipated by the model. Therefore, although element deletion is intrinsically mesh size dependent, this effect is minimal in this problem.

3.2. Comparison with experiments

The survival probability of a bundle was obtained with 100 Monte Carlo FE simulations, and these predictions are compared to experiments on microcomposites in Fig. 7. Results are shown for a bundle with four AS4 fibres in part (a) and for one with seven IM6 fibres in part (b). The analytical predictions from the hierarchical fibre bundle model of Pimenta and Pinho [22] are also included for comparison.

In both cases, the Monte Carlo FE simulations are slightly overestimating the measured survival probabilities, see Fig. 7. This could be due for instance to the difficulty to measure accurately the constituent properties and the bundle strength, or the fact that fibre debonding is not included in the simulations. Nevertheless, the predictions are in good agreement with experiments, therefore validating our modelling approach. There is also a good agreement between the analytical and Monte Carlo FE predictions, which is encouraging evidence supporting the hierarchical failure approach used by Pimenta and Pinho [22].

4. Conclusions

A Finite Element model was developed to investigate how stress redistribution in composites varies with the number of broken fibres in a cluster. The results showed that both the recovery length and stress concentration factor increase with increasing broken cluster size. More specifically, the relative stress increase in the fibre adjacent to the broken cluster nearly tripled (from 6% to 17%) when the number of broken fibres was increased from 1 to a representative critical cluster size of 16.

Analytical equations were developed to predict how the recovery length and stress concentration factor vary as a function of the number of broken fibres. These analytical predictions were found to be in good agreement with our Finite Element simulations for all broken cluster sizes considered. These results provide an accurate and effective representation of stress redistribution in composites, and may prove valuable for some fibre bundle models.

Finally, our Finite Element model was extended to predict the survival probability of fibre bundles using Monte Carlo simulations. Our approach of modelling the fibres with truss elements and meshing the matrix with continuum elements increased significantly the computational efficiency and allowed direct comparison with experiments on microcomposites. The survival probabilities predicted by these Monte Carlo simulations were found to be in good agreement with experimental data therefore validating our modelling approach.

Acknowledgments

This work was supported by the Engineering and Physical Sciences Research Council [grant number EP/M002500/1].

References

[1] Pimenta S. Fibre failure modelling. In: Camanho PP, Hallett SR, editors. Numerical modelling of failure in advanced composite materials; chap. 8. Woodhead Publishing; 2015, p. 193–224.

[2] Swolfs Y, Verpoest I, Gorbatikh L. A review of input data and modelling assumptions in longitudinal strength models for unidirectional fibre-reinforced composites. Compos Struct 2016;150:153–72.

[3] Hedgepeth JM. Stress concentrations in filamentary structures. Tech. Rep. NASA-TN-D-882; NASA Langley Research Center; Hampton, VA; 1961.

[4] Wagner HD, Eitan A. Stress concentration factors in two-dimensional composites: effects of material and geometrical parameters. Compos Sci Technol 1993;46(4):353–62.

[5] Hedgepeth JM, Van Dyke P. Local stress concentrations in imperfect filamentary composite materials. J Compost Mater 1967;1(3):294–309.

[6] Goree JG, Gross RS. Stresses in a three-dimensional unidirectional composite containing broken fibers. Eng Fract Mech 1980;13(2):395–405.

[7] Goree JG, Gross RS. Analysis of a unidirectional composite containing broken fibers and matrix damage. Eng Fract Mech 1980;13(3):563–78.

[8] Beyerlein IJ, Phoenix SL. Stress concentrations around multiple fiber breaks in an elastic matrix with local yielding or debonding using quadratic influence superposition. J Mech Phys Solids 1996;44(12):1997–2039.

[9] van den Heuvel PWJ, Wubbolts MK, Young RJ, Peijs T. Failure phenomena in two-dimensional multi-fibre model composites: 5. A finite element study. Compos Part A 1998;29:1121–35.

[10] Fiedler B, Klisch A, Schulte K. Stress concentrations in multiple fibre model composites. Compos Part A 1998;29(910):1013–9.

[11] Landis CM, McMeeking RM. Stress concentrations in composites with interface sliding, matrix stiffness and uneven fiber spacing using shear lag theory. Int J Solids Struct 1999;36(28):4333–61.

[12] Blassiau S, Thionnet A, Bunsell AR. Micromechanisms of load transfer in a unidirectional carbon fibre-reinforced epoxy composite due to fibre failures. Part 1: micromechanisms and 3D analysis of load transfer: the elastic case. Compos Struct 2006;74(3):303–18.

[13] Blassiau S, Thionnet A, Bunsell AR. Micromechanisms of load transfer in a unidirectional carbon fibre-reinforced epoxy composite due to fibre failures. Part 2: influence of viscoelastic and plastic matrices on the mechanisms of load transfer. Compos Struct 2006;74(3):319–31.

[14] Blassiau S, Thionnet A, Bunsell AR. Three-dimensional analysis of load transfer micromechanisms in fibre/matrix composites. Compos Sci Technol 2009;69(1):33–9.

[15] Xia Z, Okabe T, Curtin WA. Shear-lag versus finite element models for stress transfer in fiber-reinforced composites. Compos Sci Technol 2002;62(9):1141–9.

[16] van den Heuvel PWJ, Goutianos S, Young RJ, Peijs T. Failure phenomena in fibre-reinforced composites. Part 6: a finite element study of stress concentrations in unidirectional carbon fibre-reinforced epoxy composites. Compos Sci Technol 2004;64(5):645–56.

[17] Nedele MR, Wisnom MR. Three-dimensional finite element analysis of the stress concentration at a single fibre break. Compos Sci Technol 1994;51(4):517–24.

[18] Swolfs Y, McMeeking RM, Verpoest I, Gorbatikh L. Matrix cracks around fibre breaks and their effect on stress redistribution and failure development in unidirectional composites. Compos Sci Technol 2015;108:16–22.

[19] Swolfs Y, Gorbatikh L, Romanov V, Orlova S, Lomov SV, Verpoest I. Stress concentrations in an impregnated fibre bundle with random fibre packing. Compos Sci Technol 2013;74:113–20.

[20] Aroush DRB, Maire E, Gauthier C, Youssef S, Cloetens P, Wagner HD. A study of fracture of unidirectional composites using in situ high-resolution synchrotron X-ray microtomography. Compos Sci Technol 2006;66(10):1348–53.

[21] Scott AE, Mavrogordato M, Wright P, Sinclair I, Spearing SM. In situ fibre fracture measurement in carbon-epoxy laminates using high resolution computed tomography. Compos Sci Technol 2011;71(12):1471–77.

[22] Pimenta S, Pinho ST. Hierarchical scaling law for the strength of composite fibre bundles. J Mech Phys Solids 2013;61(6):1337–56.

[23] Beyerlein IJ, Phoenix SL. Statistics of fracture for an elastic notched composite lamina containing Weibull fibers - Part I. Features from Monte-Carlo simulation. Eng Fract Mech 1997;57(23):241–65.

[24] Curtin WA, Takeda N. Tensile strength of fiber-reinforced composites: I. Model and effects of local fiber geometry. J Compost Mater 1998;32(22):2042–59.

[25] Swolfs Y, Morton H, Scott AE, Gorbatikh L, Reed PAS, Sinclair I, et al. Synchrotron radiation computed tomography for experimental validation of a tensile strength model for unidirectional fibre-reinforced composites. Compos Part A 2015;77:106–13.

[26] Rosen BW. Tensile failure of fibrous composites. AIAA J 1964;2(11):1985–91.

[27] Curtin WA. Theory of mechanical properties of ceramic-matrix composites. J Am Ceram Soc 1991;74(11):2837–45.

[28] Harlow GD, Phoenix SL. The chain-of-bundles probability model for the strength of fibrous materials I: analysis and conjectures. J Compos Mater 1978;12(2):195–214.

[29] Harlow DG, Phoenix SL. The chain-of-bundles probability model for the strength of fibrous materials II: a numerical study of convergence. J Compos Mater 1978;12(3):314–34.

[30] Zhou SJ, Curtin WA. Failure of fiber composites: a lattice green function model. Acta Metall Mater 1995;43(8):3093–104.

[31] Okabe T, Takeda N, Kamoshida Y, Shimizu M, Curtin WA. A 3D shear-lag model considering micro-damage and statistical strength prediction of unidirectional fiber-reinforced composites. Compos Sci Technol 2001;61(12):1773–87.

[32] Tavares RP, Melro AR, Bessa MA, Turon A, Liu WK, Camanho PP. Mechanics of hybrid polymer composites: analytical and computational study. Comput Mech 2016;57(3):405–21.

[33] Beyerlein IJ, Phoenix SL. Statistics for the strength and size effects of microcomposites with four carbon fibers in epoxy resin. Compos Sci Technol 1996;56(1):75–92.

[34] Kazanci M. Carbon fiber reinforced microcomposites in two different epoxies. Polym Test 2004;23(7):747–53.

[35] Pimenta S, Pinho ST. An analytical model for the translaminar fracture toughness of fibre composites with stochastic quasi-fractal fracture surfaces. J Mech Phys Solids 2014;66:78–102.

[36] Sneddon IN. The distribution of stress in the neighbourhood of a crack in an elastic solid. Proc R Soc A 1946;187(1009):229–60.

[37] Timoshenko S, Goodier JN. Theory of elasticity. 2 ed.; McGraw-Hill; 1951.

[38] Okabe T, Takeda N. Elastoplastic shear-lag analysis of single-fiber composites and strength prediction of unidirectional multi-fiber composites. Compos Part A 2002;33(10):1327–35.

[39] Okabe T, Takeda N. Size effect on tensile strength of unidirectional CFRP composites — experiment and simulation. Compos Sci Technol 2002;62(15):2053–64.

[40] Okabe T, Sekine H, Ishii K, Nishikawa M, Takeda N. Numerical method for failure simulation of unidirectional fiber-reinforced composites with spring element model. Compos Sci Technol 2005;65(6):921–33.

[41] Okabe T, Ishii K, Nishikawa M, Takeda N. Prediction of tensile strength of unidirectional CFRP composites. Adv Compos Mater 2010;19(3):229–41.

Table 1: Material properties employed in the Finite Element simulations to analyse stress redistribution. These are representative of the T800H/3631 carbon fibre prepreg.

Material property	Value	Reference
Fibre Young's modulus E_f	294 GPa	[39]
Matrix shear modulus G_m	1.2 GPa	[39]
Matrix Poisson's ratio ν_m	0.40	[19]
Matrix shear yield strength τ_y	52.4 MPa	[39]

Table 2: Material properties employed in the Monte Carlo Finite Element simulations.

	Fibre properties						Matrix properties		
Fibre/Epoxy	ϕ (μm)	V_f	E_f (GPa)	σ_0 (GPa)	m	L_0 (mm)	G_m (MPa)	ν_m	τ_y (MPa)
AS4/DER 331+732	6.85	0.70	231	4.493	4.8	10	179.3	0.4	4.0
IM6/DER 331	5.63	0.56	280	5.283	5.4	10	604.5	0.4	46.6

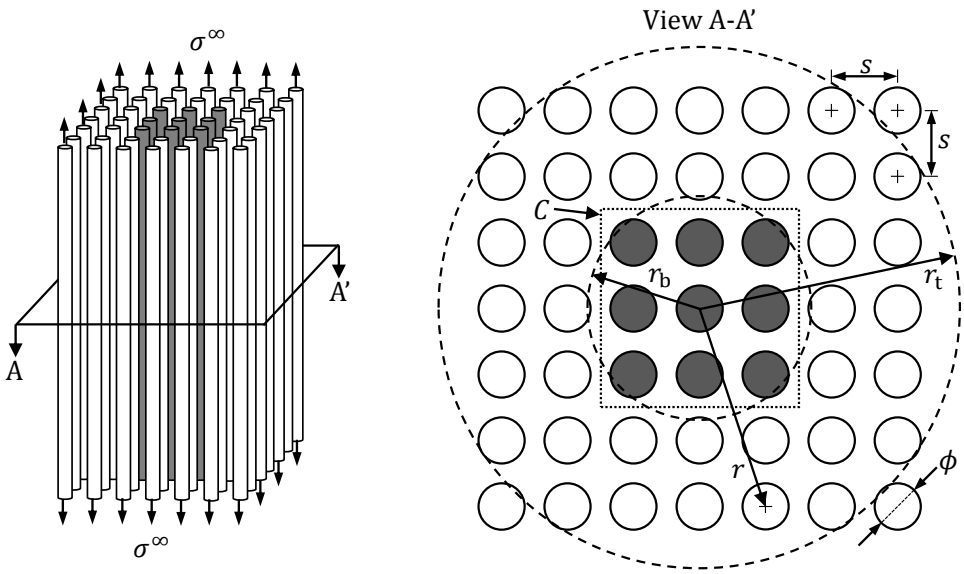

Figure 1: Fibre bundle loaded in tension by a remote fibre stress σ^∞. The bundle has n_t fibres and contains, at its centre, a cluster of n_b broken fibres highlighted in grey. All breaks are contained in the A-A' plane. Quantities used in our analytical model are also shown: the assumed shear-lag perimeter C and the equivalent radii of the bundle r_t and of the broken cluster r_b.

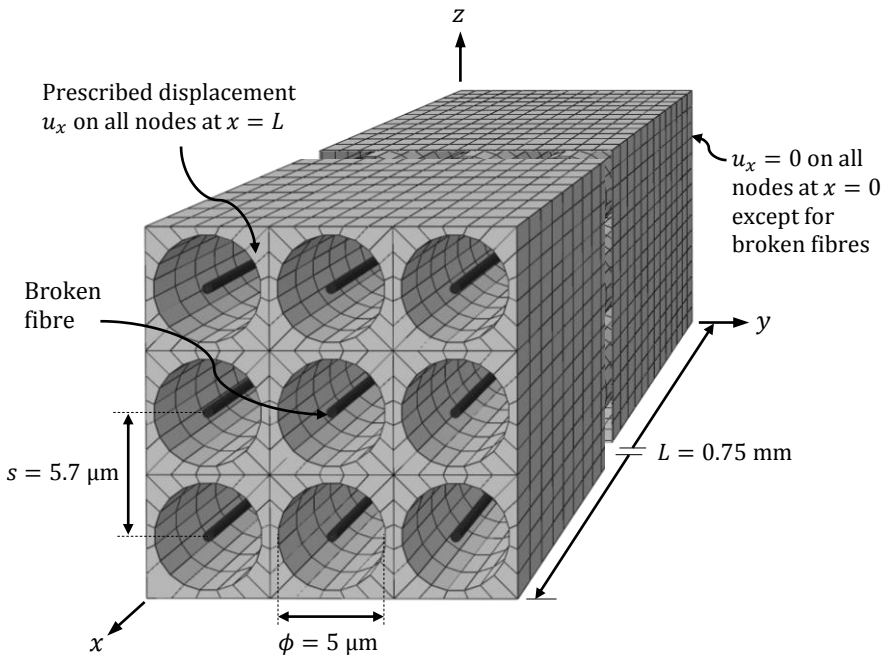

Figure 2: Finite Element model developed to analysed stress redistribution: a bundle with $n_{\mathrm{t}} = 9$ fibres containing $n_{\mathrm{b}} = 1$ broken fibre is shown here as an example. The fibres, modelled with truss elements, are perfectly bonded to the matrix, meshed with continuum elements, using constraint equations.

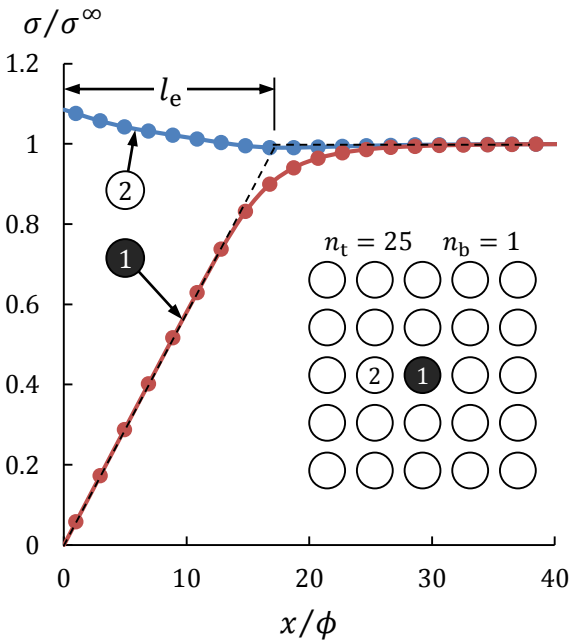

Figure 3: Stress profiles along the length of the fibres: the normalised longitudinal stress σ/σ^∞ is shown as a function of the normalised distance from the fibre break plane x/ϕ for the broken fibre (labelled 1) and its closest neighbour (labelled 2). Results are shown for a remote tensile fibre stress $\sigma^\infty = 4.3\,\text{GPa}$, and the recovery length l_e is identified.

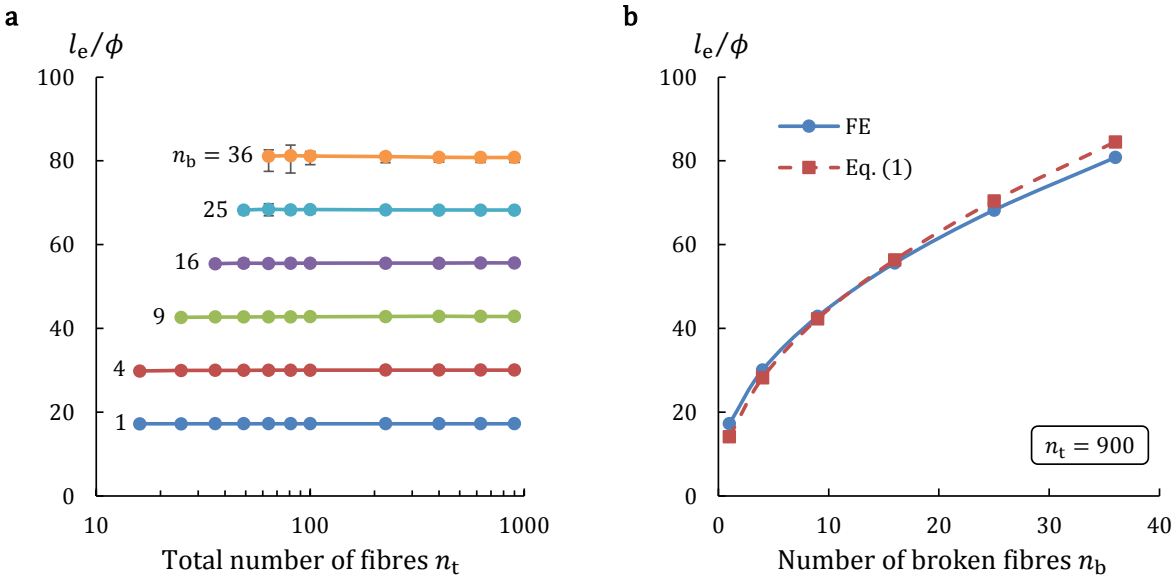

Figure 4: Normalised recovery length l_e/ϕ as a function of (a) the total number of fibres in the bundle n_t and (b) the number of broken fibres n_b for a bundle with $n_t = 900$ fibres. Results are shown for a remote tensile fibre stress $\sigma^\infty = 4.3\,\text{GPa}$.

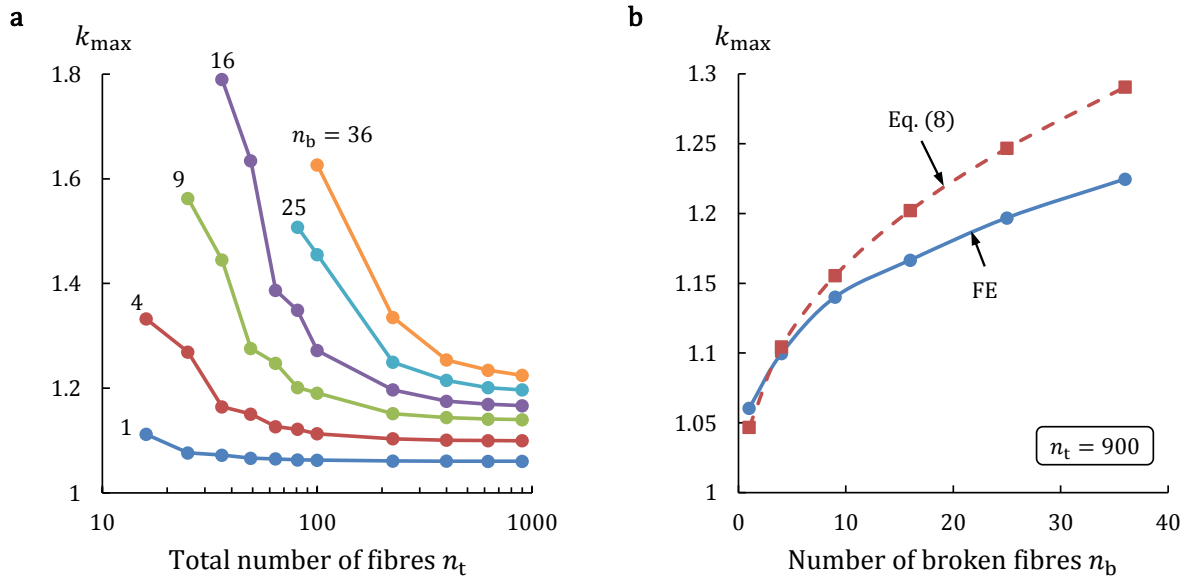

Figure 5: Maximum stress concentration factor $k_{\max}$ as a function of (a) the total number of fibres in the bundle n_t and (b) the number of broken fibres n_b for a bundle with $n_t = 900$ fibres.

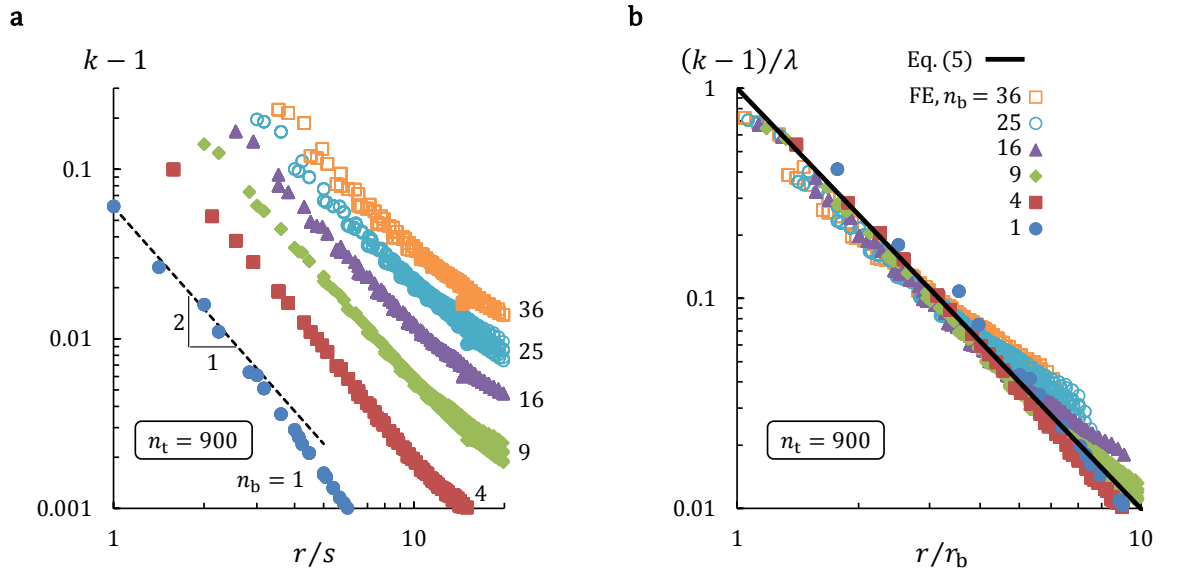

Figure 6: (a) Stress concentration factor k as a function of the normalised distance from the broken cluster r/s. (b) The same FE results are plotted with a different normalisation and compared to the predictions of Eq. (5). In both parts, results are shown for a bundle with $n_t = 900$ fibres and for selected number of broken fibres n_b.

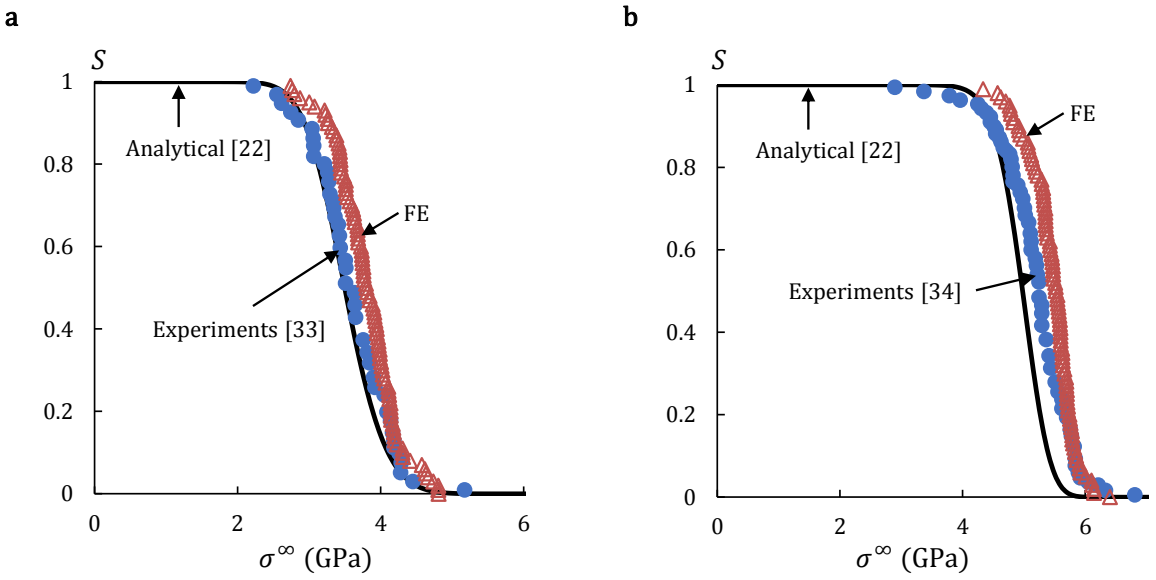

Figure 7: Survival probability S as a function of the remote tensile fibre stress σ^{∞} for microcomposites with: (a) four AS4 carbon fibres in a blend of DER 331 and 732 epoxy (50:50) and (b) seven IM6 carbon fibres in a DER 331 epoxy. Monte Carlo FE predictions are in good agreement with experimental [33, 34] and analytical [22] results.